Electrochemical Differentiation and TOF-SIMS Characterization of Thiol-Coated Gold Features for (Bio)chemical Sensor Applications

Michal Tencer,[a,b,z] **Heng-Yong Nie,**[c,z] **and Pierre Berini**[a,d,e,z]

[a]*School of Information Technology and Engineering and* [e]*Department of Physics, University of Ottawa, Ottawa, Ontario K1N 6N5, Canada*
[b]*MST Consulting, Ottawa, Ontario K2H 8T3, Canada*
[c]*Surface Science Western, University of Western Ontario, London, Ontario N6A 5B7, Canada*
[d]*Spectalis Corporation, Ottawa, Ontario K2K 2P4, Canada*

A method to chemically differentiate small closely spaced lithographically defined Au features with different thiol-based self-assembled monolayers (SAMs) was developed. The key step in the method is the reductive electrochemical desorption of a SAM from a specific Au feature without affecting SAMs on neighboring Au features by simultaneously controlling their potentials with a multichannel potentiostat. The method is demonstrated by chemically differentiating the arms of a Au plasmonic Mach–Zehnder interferometer such that the arms have different affinities toward an analyte, thus rendering the interferometer useful for (bio)chemical sensing. The simultaneous presence of a poly(ethylene glycol)-terminated SAM on one arm, and of a biotin-terminated SAM on the other, was verified by imaging with time-of-flight secondary ion mass spectrometry (TOF-SIMS) and phase-shift atomic force microscopy. The method can be applied generally to chemically differentiate a large number of electrically isolated Au features simultaneously, leading to low cost wafer-scale functionalization of (bio)chemical sensors and other devices.
© 2009 The Electrochemical Society. [DOI: 10.1149/1.3242308] All rights reserved.

When designing and making chip-scale laboratories, especially for biosensing applications, a need arises for chemical differentiation of small closely spaced structural features of various shapes and sizes, having dimensions on the order of a micrometer or less, and often separated by similarly small distances. An example of a sensing structure where this occurs is the plasmonic Mach–Zehnder interferometer (MZI) implemented using metal stripes and destined to operate with long-range surface plasmon polaritons.[1-4] Such sensors hold the promise of label-free detection with high sensitivity and a low detection limit.[1,3,5-7]

Figure 1a shows a sketch of such MZIs,[1,2] and Fig. 1b shows a microscope image of an MZI fabricated from 25–35 nm thick Au stripes. This design has two 5 μm wide arms separated by tens of micrometers, 100×100 μm electrical contact pads suitable for probing, and four 2 μm long gaps for electrical isolation (the effect of such a gap is optically negligible[8]). In this configuration, any differential adsorption between the MZI arms results in a change in signal intensity at the output.

The MZI arms are closely spaced Au features that should be chemically differentiated to render one of them prone to specific adsorption of the target analyte, e.g., a protein, and the other blocked from any specific or nonspecific adsorption. Thiol-based self-assembled monolayers (SAMs), which can easily be formed on gold, can be utilized to achieve these functions. For example, hydrophobic SAMs based on simple alkanethiols $CH_3(CH_2)_n SH$ promote nonspecific adsorption of proteins, while those formed with poly(ethylene glycol) (PEG)-terminated thiols $HO(C_2H_4O)_m(CH_2)_n SH$ and other hydrophilic SAMs prevent this process.[9-11] Proteins also adsorb nonspecifically on bare gold,[12] but this process is not kinetically or thermodynamically[13] well defined and is usually irreversible due to denaturation.[12,14] Thus, to achieve sensing, we need to have one MZI arm coated with an adsorption resistant SAM and the other with a SAM promoting specific adsorption of the analyte of interest. High specificity can be attained through, e.g., antigen–antibody interaction, where the antibody is immobilized on the SAM.[15,16] The high specificity of the biotin/streptavidin system may also be utilized.[17,18]

Performing selective chemistries on the Au MZI arms (as shown in Fig. 1) or on other micrometer-sized closely spaced metallic features on a flat solvophilic surface presents a challenge because any droplet that can be practically deposited will be much larger than the distance between the arms and 2 orders of magnitude larger than the arms' width. For instance, a sessile 0.1 μL water droplet having a volume $V = 0.1$ μL and a contact angle of 90° has a footprint of diameter $d = (12V/\pi)^{1/3} = 726$ μm. Additionally, thiol SAMs are typically formed using organic solvents that wet polar substrates, especially when they are cleaned with UV ozone, plasma, or Piranha solution, leading to uncontrollable spreading. Rinsing the structures without cross contamination presents another set of issues. To overcome these challenges, we have previously devised a method where the solution is confined between the surface to be treated and an appropriately shaped guide having a solvophilic surface, which is then positioned over the feature to be coated.[19] The method was successfully applied to deposit bovine serum albumin on bare Au MZI arms.[2,19] However, it is not easily scaled to simultaneously treat multiple features in a wafer-scale process.

Rather than going for expensive methods of microspotting such as microcontact printing or ink jetting, we decided to explore electrochemical desorption of SAMs[20-25] as a methodology for chemical differentiation of small Au features, in this case, MZI arms. A previous paper,[25] using large Au features on a dielectric substrate separated by a scribed 45 μm wide groove, showed that reductive desorption of a dodecanethiol-based SAM can be performed toposelectively on one feature without affecting the other. A SAM on Au has a range of potentials over which it is stable and beyond which it desorbs.[25] Both reductive ($AuSR + e^- \rightarrow Au^0 + RS^-$) and oxidative ($AuSR + xH_2O \rightarrow Au^0 + RSO_x + ne^-$) desorption can be employed, but the latter has to be applied with more caution because in the presence of complexing ions (e.g., Cl$^-$), it may lead to loss of gold.[25]

In this paper, a process leading to a Au MZI, in which one arm is coated with a protein-adsorption-blocking PEG-terminated SAM and the other arm is coated with a biotin-terminated SAM that promotes a specific adsorption of avidin, streptavidin, and their complexes, is described. The process, which utilizes reductive desorption of a SAM from gold as the key step, is applicable to any electrically isolated gold structures on a chip. The important issues of the relative electrical resistances between neighboring structures (here, the arms of an MZI) and between the structures and the counter electrode in an electrolyte solution are discussed in detail as they are related to the potentials that must be applied. An example of a proposed layout to enable wafer-scale processing is also described.

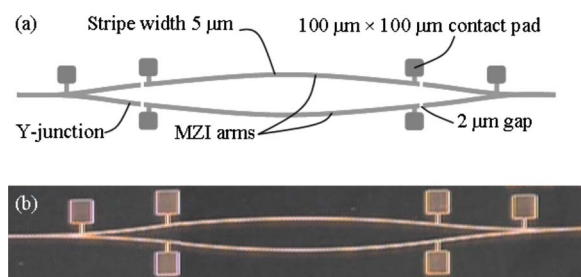[z] E-mail: mtencer@site.uottawa.ca; hnie@uwo.ca; berini@site.uottawa.ca

Figure 1. (Color online) (a) Sketch of an equal arm plasmonic MZI supporting LRSPPs featuring electrical contact pads and electrical isolation gaps. The maximum distance between the MZI arms ranges from 90 to 240 µm depending on the design. (b) Microscope image of an MZI fabricated from 25 nm thick Au stripes.

Two surface analysis techniques were applied to validate the process developed: Time-of-flight secondary ion mass spectrometry (TOF-SIMS)[26-28] was used to reveal the presence of the molecules by detecting characteristic ion fragments, and phase-shift imaging in atomic force microscopy (PS-AFM)[29-31] was used to detect differences in the viscoelastic properties of surfaces with different SAMs.

Theoretical: Resistances and Potentials

The resistances between different electrodes of the electrochemical cell determine how tightly their potentials must be controlled; the electrodes consist of the MZI arms and the counter electrode. Let us assume that only the MZI arm to undergo desorption is negatively biased, while the other one is not controlled. The whole system, including a counter electrode, is immersed in an electrically conductive medium, i.e., an electrolyte. We need to know how the voltage drop between the arms compares to the voltage drop between the biased arm and the counter electrode. If the former is much smaller than the latter, then both arms have a similar potential and so are not electrically differentiated. The situation is sketched in Fig. 2. From the equivalent circuit in Fig. 2, and assuming that $R_{E1} = R_{E2} \equiv R_E$ (because MZI arms B and C are close to each other and far from counter electrode A), the ratio of the voltage drop V_0 between the arms to the total voltage drop V is

$$\frac{V_0}{V} = \frac{I_2 R_0}{V} = \frac{R_0}{R_E + R_0} \qquad [1]$$

Thus, if the resistance R_0 between arms B and C is much smaller than the resistance R_E between an arm and counter electrode A, they will have a similar potential and the SAM will be dislodged from both arms.

To estimate R_0, we consider the simplified MZI sketched in Fig. 3a and its equivalent resistive circuit, as seen from the midpoint of the MZI arms, sketched in Fig. 3b. By inspection, R_0 is given by

$$\frac{1}{R_0} = \frac{1}{R_D} + \frac{1}{R_G + \frac{1}{2}R_{L2} + \frac{1}{2}R_{L1}} \qquad [2]$$

where R_D and R_G are resistances through the electrolyte as indicated. The resistances R_{L1} and R_{L2} are given by

$$R_{L1,L2} = \rho_{Au} \frac{L_{1,2}}{wt} \qquad [3]$$

where $\rho_{Au} = 2.21 \times 10^{-8}$ Ω m is the resistivity of Au. Assuming typical values for the lengths $L_1 = 3000$ µm and $L_2 = 800$ µm, the stripe width $w = 5$ µm, and its thickness $t = 25$ nm yields $R_{L1} = 530$ Ω and $R_{L2} = 141$ Ω.

The resistance through the electrolyte R_D can be modeled as the resistance between two long parallel wires immersed in a conductive medium because the metal stripes are narrow and thin compared to their length and separation ($w, t \ll D, L_1$). Two wires in an electrolyte are often used in conductance measurements of biological flu-
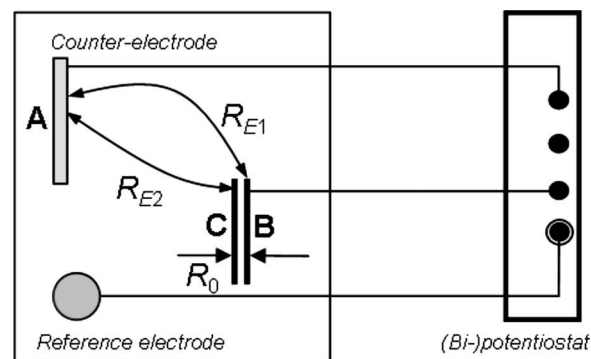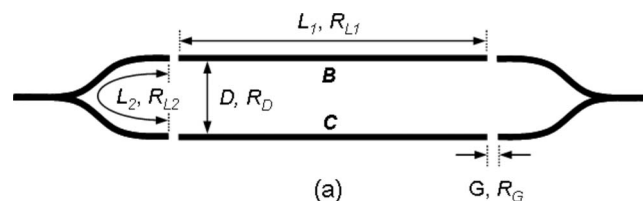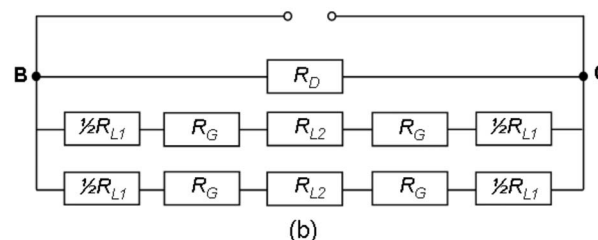

(a)
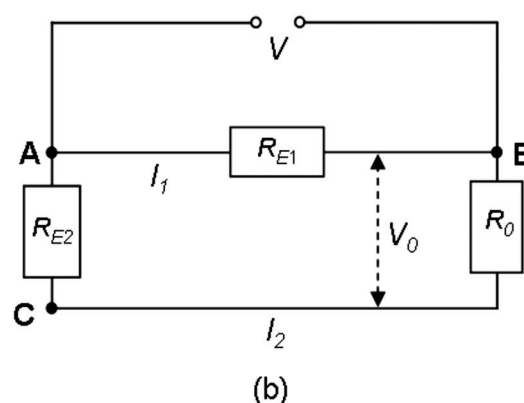
(b)

Figure 2. (a) Electrochemical desorption with single potential control: A, the counter electrode; B, the arm to undergo desorption; and C, the arm to stay unchanged. (b) Equivalent dc circuit for this configuration.

ids, but these are typically calibrated empirically with solutions of known conductance yielding a "cell constant." However, for such systems, an analogy to electrostatics[32] can be used, as in the areas of glass technology[33,34] and anodic corrosion protection in soil.[35,36] In this latter field, easy-to-use formulas were derived, which can be used to determine R_D. Thus, correcting for the fact that only half the space is available for conduction, the resistance between the arms through an electrolyte with resistivity ρ_{el} can be estimated as

(a)

(b)

Figure 3. (a) Geometrical features and resistances of an idealized MZI similar to that in Fig. 1. (b) Equivalent dc circuit, as seen from the midpoint of the MZI arms.
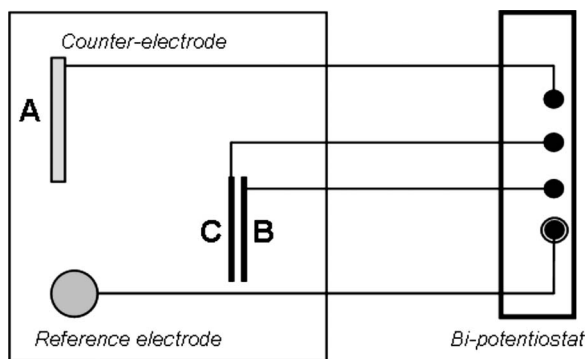
Figure 4. Electrochemical desorption configuration with dual potential control: A, the counter electrode; B, the arm to undergo desorption, and C, the arm to stay unchanged.

Figure 5. Structure of the thiols used in this study: **I**, tri(ethylene glycol) mono-11-mercaptoundecyl ether; **II**, biotin-terminated undecylthiol; and **III**, dodecanethiol.

$$R_D = \frac{\rho_{el}}{\pi L_1}\left[\sinh^{-1}\frac{2L_1}{D} - \sqrt{1+\left(\frac{D}{2L_1}\right)^2} + \frac{D}{2L_1}\right]^{-1} \quad [4]$$

For a typical electrolyte of 0.1 N NaCl, $\rho_{el} = 1100$ Ω m.[37] Assuming typical values for the length $L_1 = 3000$ μm and the arm separation $D = 100$ μm yields $R_D = 31$ kΩ. With somewhat less accuracy, the same equation is used to estimate the resistance in the gap by replacing L_1 with w and D with G

$$R_G = \frac{\rho_{el}}{\pi w}\left[\sinh^{-1}\frac{2w}{G} - \sqrt{1+\left(\frac{G}{2w}\right)^2} + \frac{G}{2w}\right]^{-1} \quad [5]$$

For $G = 2$ μm, this yields $R_G = 47$ MΩ. This value is much larger than R_{L1} and R_{L2} and so dominates in Eq. 2.

Thus, the total resistance between the MZI arms, as calculated from Eq. 2, is $R_0 = 31$ kΩ. Assuming that the counter electrode has similar dimensions to an MZI arm but is located much further in the electrochemical cell, say, 2 cm away, it yields $R_E = 784$ kΩ (computed via Eq. 4, assuming $D = 2$ cm and $L_1 = 3000$ μm). Therefore, according to Eq. 1, the voltage drop between the MZI arms is only ca. 3.7% of the total voltage drop, which means that if we apply a SAM desorbing potential to one arm without controlling the potential on the other arm, then the other arm also undergoes desorption. (Desorption of other neighboring MZIs or features on the wafer may also occur if they are situated close to the MZI being treated.) This necessitates an independent simultaneous control of both MZI arms, as shown in Fig. 4. However, in systems where features are larger and the distance between them and the counter electrode is much smaller, controlling only the potential of a single feature should be adequate, as has been shown for microarrays.[38,39]

Another consideration pertains to the electrical resistance between MZI arms through the substrate. If the gold MZI structure is deposited directly on silicon (or on the native oxide) rather than on a thick dielectric layer, then the resistance between the arms could be very low. In this case, a substantial shunt current may flow between the arms, resulting in a situation where the actual potentials of the electrodes differ considerably from the ones indicated by the potentiostat.[25] In practice, different desorption potentials should be established for the low resistance between the MZI arms for a given potentiostat/cell system.

Finally, because the chemistry on the Y-junctions, and thus their potentials, is also controlled, we must ensure that the electric field in the 2 μm gaps is small compared to the dielectric breakdown field. Where the Y-junctions have the same potential as one of the MZI arms, the electric field in the gap between a junction and the other arm is $E = \Delta V/G$. With the typical potential difference between the arms being ca. 2 V, the electric field in a 2 μm gap would be 1 MV/m. This is still below the dielectric strength of pure water (3.2 MV/m) or air (3 MV/m), so dielectric breakdown is not expected.
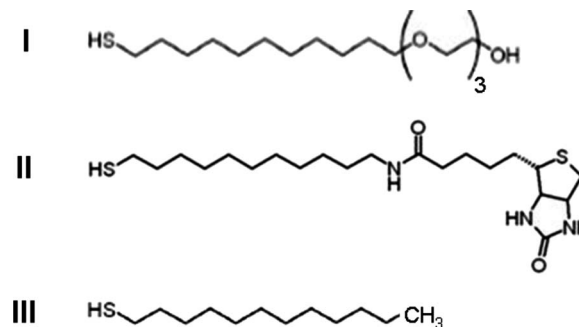
Experimental

Materials.— 1-Dodecanethiol, $HS(CH_2)_{11}CH_3$, henceforth referred to as thiol **III** (≥98%, Arkema Inc.), triethylene glycol mono-11-mercaptoundecyl ether, $HS(CH_2)_{11}(C_2H_4O)_3OH$ (or $C_{17}H_{36}O_4S$ emp. form.), henceforth referred to as thiol **I**, and phosphate buffer (PB) solution (0.1 M, pH 7.5) were purchased from Sigma-Aldrich Canada Ltd. Deionized (DI) water was prepared from distilled water using a Zenopure Quatra 90 LC system, and the eluate with a resistivity ≥17 MΩ cm was collected. Semiconductor grade 2-propanol (Puranal) was obtained from Riedel–de Haën. The biotin-terminated undecylthiol $HS(CH_2)_{11}NHCOC_9H_{15}N_2OS$ (or $C_{21}H_{39}N_3O_2S_2$ emp. form.), henceforth referred to as thiol **II**, was purchased from ProChimia Surfaces, Sp. z o.o., Sopot, Poland. The thiol structures are shown in Fig. 5.

Sample preparation.— Thiols **I** and **III** were used as 2 mM solutions in isopropanol. Thiol **II** was used as a 2 mM solution in a 75:25 v/v ethanol/dimethyl sulfoxide (DMSO) mixture, and any undissolved thiol was filtered off. The Au surfaces were degreased with 2-propanol, rinsed with DI water, and placed in a Novascan PSD-UV UV-ozone cleaner (5 min UV irradiation followed by 20 min ozone action). The dies were then immersed in a thiol solution for a period of time (as described below), rinsed thoroughly with isopropanol and water, and allowed to dry. Henceforth, SAMs formed from thiols **I**, **II**, and **III** on gold are called SAM **I**, SAM **II**, and SAM **III**, respectively.

Substrates and structures.— Large area samples were cleaved from p-type Si wafers bearing a 30 nm thick layer of Au on 4.5 nm of Cr (blanket coverage, vacuum-evaporated) and were used to determine the SAM desorption potentials. The MZI structures used (Fig. 1) were defined from 25 nm thick, 5 μm wide Au stripes, on a thin Cr adhesion layer, a 15 μm thick thermally oxidized SiO_2 layer, and Si wafers, and were fabricated using lift-off and vacuum evaporation.

Electrochemistry and electrical measurements.— The electrolysis experiments were performed in 0.1 M PB (pH 7.5) with a Pine Research AFCBP1 bipotentiostat using a four-electrode configuration (one reference, two working electrodes, and one counter electrode). The counter electrode was a platinum wire. A double-junction Ag/AgCl reference electrode was used. All potentials are reported with respect to this reference. DC resistances were measured with a Keithley 2000 multimeter in a two-wire configuration. The 100 × 100 μm pads were electrically contacted with Quater 20235 dc probes controlled with Quater XYZ 5000 TRM positioners under a stereomicroscope. After the process, the samples were rinsed in a jet of water and isopropanol and were allowed to dry.

Analysis.— Contact angles were measured using a VCA Optima goniometer from AST Products Inc. At least three sessile droplets of

DI water were produced each time, and the average of the left and right angles and their standard deviations were calculated.

TOF-SIMS on the MZIs was performed using an ION-TOF (GmbH) TOF-SIMS IV equipped with a Bi liquid metal ion source. A 25 keV Bi_3^+ cluster primary ion beam pulsed at 10 kHz with a pulse width of 12 ns and a target current of ∼1 pA was used to bombard the sample surface to generate secondary ions. The secondary ions were extracted from the sample surface, mass separated, and detected via a reflectron-type TOF analyzer, allowing parallel detection of ion fragments having a mass/charge (m/z) ratio of up to 900 within each cycle (100 μs). For thiols **I** and **II**, we found the negative secondary ion spectra to be more informative than the positive ones for the purpose of molecular identification; thus, only negative secondary ion mass spectra are discussed in this study. A pulsed low energy (∼18 eV) electron flood was used to neutralize sample charging; the current was maintained below ∼20 μA maximum to avoid sample damage. Full spectra were collected at 256 × 256 pixels over a scanned area (352 × 352 μm). Ion images were rendered by plotting their intensity against the pixels where the mass spectra were collected.

AFM.— The gaps of 2 μm separating Au stripes that were either a control (i.e., bare Au) or bearing SAMs **I** and **II** were imaged using the dynamic force mode of a Park Systems XE-100 AFM. A silicon cantilever having a nominal spring constant of 40 N/m and a tip radius of 10 nm was used. In the dynamic force mode, the tip was made to oscillate near its resonant frequency by applying a driving ac voltage to a bimorph on which the cantilever is attached. When the tip gets close to the sample surface, the tip–sample interaction causes the oscillation amplitude to decrease. This damped amplitude is used as the feedback parameter for imaging the topography of the sample. The phase-shift angle is the phase difference between the driving voltage and the oscillation of the cantilever, as detected by a photodetector. The phase-shift angle is sensitive to tip–sample interaction,[29-31] which makes phase-shift imaging a powerful technique to differentiate materials having different mechanical, chemical, and adhesion properties.

Results and Discussion

Desorption potentials for SAM I.— The potential range for the electrochemical desorption of SAM **I** was established using water contact angle measurements. This method was used previously with SAM **III**, which is very hydrophobic, and thus was characterized with high contact angles.[25] Here, however, both SAM **I** and bare gold are hydrophilic; thus, an indirect method had to be used: The samples were first incubated with thiol **I** for 16 h and then rinsed and dried; contact angle measurements confirmed that the surfaces were very hydrophilic. The samples were then subjected to a potential for 3 min in a three-electrode configuration, washed, dried, and reincubated with thiol **III** for 5 min, and then rinsed and dried. The water contact angle was then measured. The results are plotted in Fig. 6, revealing that (*i*) SAM **I** desorbs completely at potentials <−1.6 V vs Ag/ACl and (*ii*) no desorption occurs at potentials between −1 and 0 V vs Ag/AgCl. The potentials of −1.6 and −0.3 V were therefore selected as the desorbing and stabilizing potentials, respectively.

SAMs on "polycrystalline" Au such as that used in this work do not exhibit any well-defined reductive waves.[21,25] Moreover, the surface area of the immersed dc probes largely exceeds that of the Au arms, and the solvent is strongly reduced at the pH used; thus, the measured current reflects mostly H_2 evolution from the probes rather than SAM desorption from the arms.

Process description.— It is desirable to functionalize MZIs such that, for example, one arm and both Y-junctions are coated with protein-blocking PEG-terminated thiol (thiol **I**), and the other arm is coated with biotin-terminated thiol (thiol **II**), which has a high affinity to avidine, streptavidin, and their derivatives. The process proposed to achieve this consists of (*i*) the formation of SAM **I** on
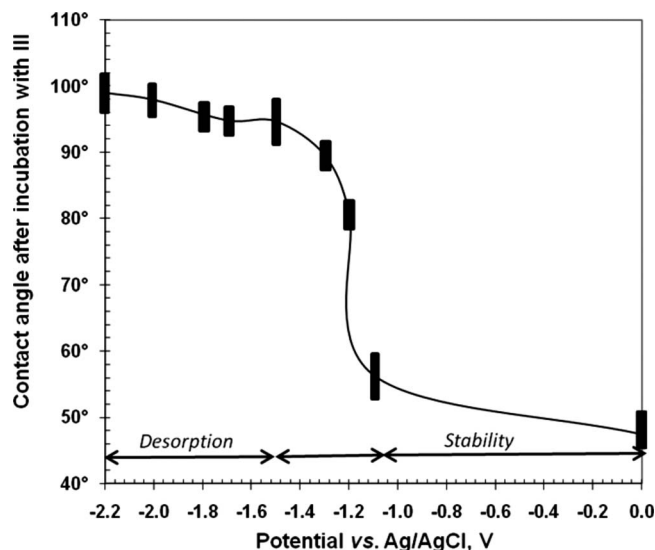
Figure 6. Potential range for the reductive desorption of SAM **I**. The water contact angles shown are after reincubation with thiol **III**. Error bars reflect standard deviations of contact angles.

the whole MZI structure through incubation, (*ii*) the selective electrochemical desorption of SAM **I** from one arm but not from the other arm or the Y-junctions, and (*iii*) the formation of SAM **II** on the desorbed arm through a short reincubation with thiol **II**, minimizing exchange with thiol **I** on the other areas of the MZI. Specifically, the process consisted of applying the following steps (also depicted by A–D in Fig. 7).

A. The dc resistance between both contact pads attached to each MZI arm was measured to assess the structural integrity of the MZI. This measurement was performed with dry samples to avoid any electrochemical process that could be introduced by the ohmmeter. The measured resistances agreed well with the expected values.

B. The sample was incubated in 2 mM thiol **I** solution in isopropanol for 16 h, rinsed in a jet of isopropanol and water, and then dried.

C. The sample was placed in the electrochemical cell. One of the pads of the left (west) MZI arm was contacted with a dc probe connected to one terminal of the bipotentiostat, while one of the pads of the right (east) arm was contacted with a dc probe connected to another terminal of the bipotentiostat. The pads of the Y-junctions were connected via dc probes to the same terminal as the east arm. Then, the cell was filled with PB, and the potential of the first terminal was set at −1.6 V vs Ag/AgCl, while that of the other
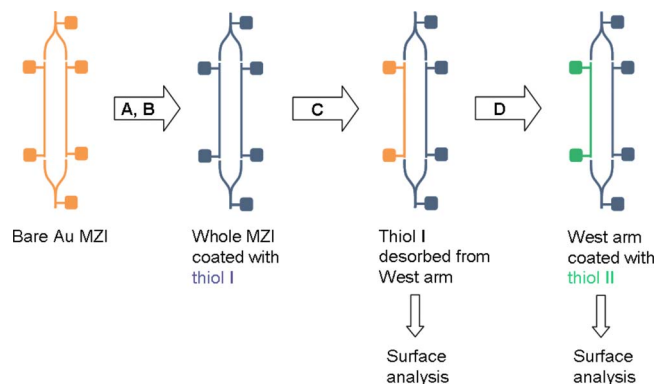
Figure 7. (Color online) Process flow for the electrochemical differentiation of MZI arms; steps A–D are described in the text.
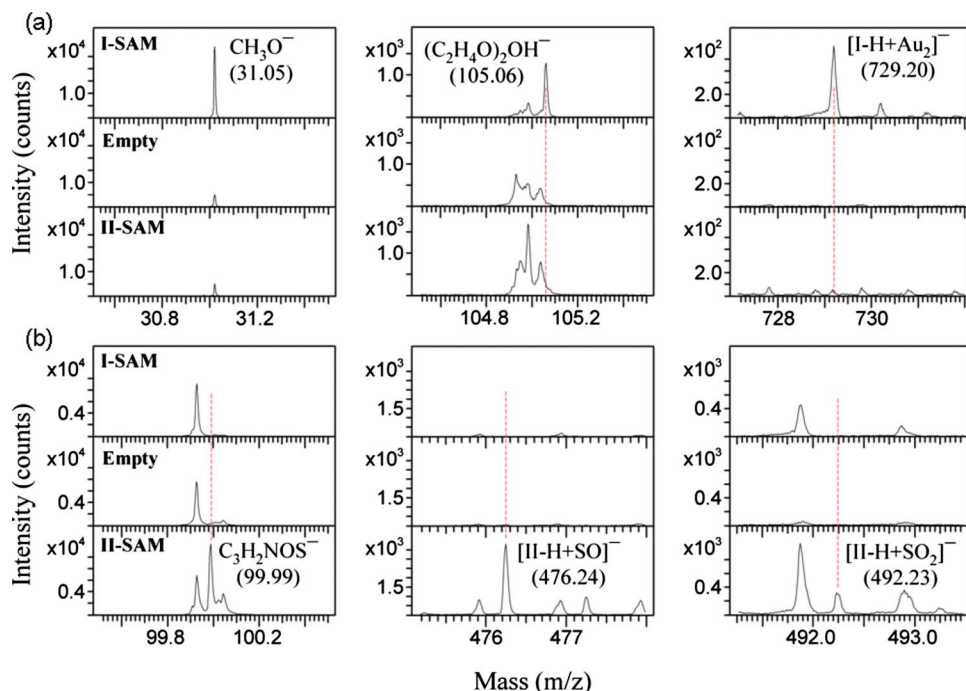
Figure 8. (Color online) Negative secondary ion mass spectra obtained on a pad covered by SAM **I**, a pad with SAM **I** removed, and a pad covered by SAM **II**. Shown are ion fragments and their mass-to-charge ratios (mass number) characteristic of thiols (a) **I** and (b) **II**, respectively.

terminal was set at -0.3 V vs Ag/AgCl (the latter is within the SAM's stability region; see Fig. 6). The electrolysis was carried out for 2 min. After the electrolysis, the die was rinsed with water and isopropanol, dried, and submitted to surface analysis.

D. Another die prepared in the same way was incubated with the thiol **II** solution for 5 min, rinsed with a 75:25 v/v ethanol/DMSO mixture, then rinsed in a jet of isopropanol and water, dried, and submitted to surface analysis. The reason for the short incubation time (which may lead to a SAM that is not fully organized) was to minimize any formation of a mixed SAM on the other arm due to a possible thiol/SAM exchange. A subsequent preliminary study of this process shows that, actually, longer incubation times could be used and that addition rather than exchange may occur.[40]

Surface analysis.— TOF-SIMS.— There are numerous common secondary ion fragments generated from SAM **I** and SAM **II** on Au by the 25 keV Bi_3^+ primary ion beam bombardment. It is thus necessary to find characteristic fragments to identify the molecules. By comparing TOF-SIMS spectra collected on bare Au and on SAM **I**–, SAM **II**–, and SAM **III**-covered Au samples, we have found that CH_3O^-, $(C_2H_4O)_2OH^-$, and $[I - H + Au_2]^-$ (where **I** $= C_{17}H_{36}O_4S$) are characteristic of thiol **I**. The spectra for the three assigned ion peaks are shown in Fig. 8a. Also shown in Fig. 8 are spectra for the "empty" Au surface (west MZI arm) where SAM **I** was removed electrochemically (step C, Fig. 7). One can see that the two characteristic ion fragments, $(C_2H_4O)_2OH^-$ and $[I - H + Au_2]^-$, disappear, confirming that SAM **I** has been electrochemically removed. However, the CH_3O^- fragment is still present on the empty Au surface albeit at a significantly decreased intensity. This weak remaining signal originates from other sources such as contamination; in our experience, it can be detected on many other samples having had no previous association with thiol **I**, where it can reach intensities as high as 10% of that of SAM **I**. We therefore treat the residual CH_3O^- signal measured on the empty Au surface as the background. The advantage of using CH_3O^- for identifying SAM **I** is its high intensity, giving a stronger contrast for small features where the total ion fragment intensity may be small.

For SAM **II**, we observe three characteristic ion peaks, $C_3H_2NOS^-$, $[II - H + SO]^-$, and $[II - H + SO_2]^-$ (where **II** $= C_{21}H_{39}N_3O_2S_2$), as shown in Fig. 8b. There is a rather weak $[I$

$- H + Au_2]^-$ peak on this reincubated sample, which could be due to contamination during the reincubation step (step D, Fig. 7).

Using the characteristic ion fragments described above for thiols **I** and **II**, we carried out TOF-SIMS imaging for an entire MZI to verify our electrochemical incubation process. Au-derived ions, such as Au_n^-, Au_nS^-, and Au_nSH^- ($n = 1,2,3$) do not differentiate the SAMs but provide an outline of the whole structure, as shown in Fig. 9a. The negative ion fragments characteristic of SAM **I** and SAM **II** were used to map the treated areas of the MZI after applying the process of Fig. 7. Ion peaks characteristic of (the biotin-derivative) thiol **II**, with $[II - H + SO]^-$ being the strongest contrasting species, clearly mark the "west" arm and its contact pads, as shown in Fig. 9b, while those derived from (the PEG-terminated) thiol **I**, with CH_3O^-, clearly mark the "east" arm, the Y-junctions, and their contact pads, as shown in Fig. 9c. We chose to use CH_3O^- to represent thiol **I** because $(C_2H_4O)_2OH^-$ is interfered by a shoulder of an ion fragment seen in the thiol **II** sample, and $[I - H + Au_2]^-$ is weak due to the rather small width of the Au line. This species (CH_3O^-) is much stronger on SAM **I** than on SAM **II** and so differentiates the two SAMs. We have confirmed this by mapping $[I - H + Au_2]^-$ over 100×100 μm Au pads covered by SAM **I** and SAM **II** as well as a Au pad with SAM **I** electrochemically removed because the ion intensity was stronger due to their greater area (compared to the 5 μm wide Au stripe).

AFM.— We applied PS-AFM as an alternative technique to verify the chemical differentiation of the treated MZI arms. Figure 10 shows images taken over the gap regions of two MZIs after the application of steps C and D, as sketched in Fig. 7. The lower half of the phase-shift image of Fig. 10a shows selective removal of SAM **I** from the west MZI due to electrolysis (step C, Fig. 7). In contrast, the east arm and the Y-junction were unaffected, as shown in Fig. 10b. The phase-shift angle on the SAM **I**-coated Au stripes is smaller than that on the empty Au arm, suggesting that the thiol may be softer. This agrees with observations made on an organic layer deposited on a Si substrate,[24] rubbers,[41] and biological tissues,[25] where phase-shift images show that a softer area has a smaller phase-shift angle than a harder area. More energy seems to be dissipated on a softer and a more adhesive surface from the oscillating tip.[30,42] Incubation of the sample with thiol **II** (step D, Fig. 7) leads to a further change in the surface, as shown in the lower half of the
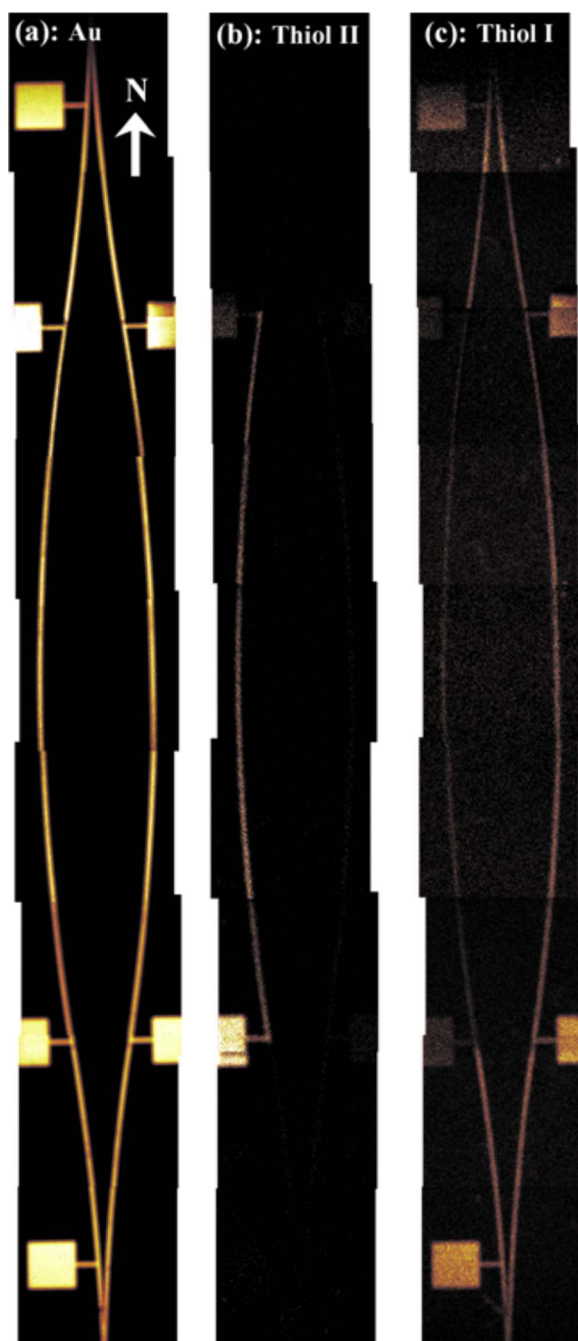
Figure 9. (Color online) TOF-SIMS mapping of an MZI after application of the full process (steps A–D, Fig. 7) using secondary ion fragments characteristic of (a) Au, (b) SAM **II**, and (c) SAM **I**.
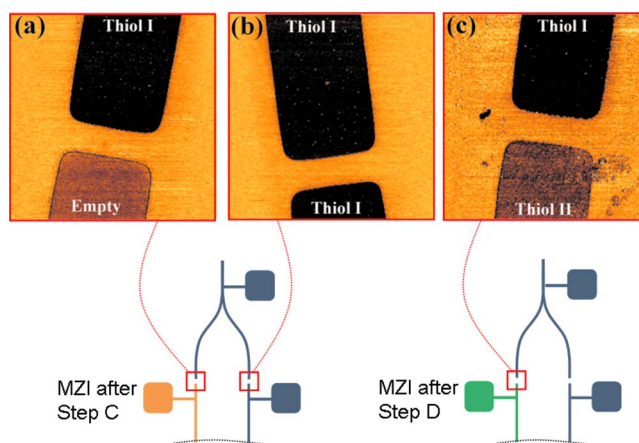

Figure 10. (Color online) AFM phase-shift images of the gap regions identified by the red square boxes on the corresponding MZI partial sketches. [(a) and (b)] MZI having undergone process steps A–D (Fig. 7). (c) MZI having undergone steps A–D (Fig. 7). The darkest areas on the images are $\sim 20°$ lower than the brightest areas (SiO$_2$ surface). The scan area for the three images is 12×12 μm.

arrangement reduces the number of contact points while allowing the west arms to share one potential and the east arms to share another. To cover large areas (say, a whole wafer), the resistance of the connections can be controlled through their width so that it remains much lower than any resistance through the electrolyte.

Conclusions

A process to chemically differentiate neighboring Au features with different thiol-based SAMs was developed and demonstrated by functionalizing a plasmonic Au MZI with PEG- and biotin-terminated thiols. The process involves two incubation steps in two thiol solutions with an intervening selective electrochemical desorption step. The first incubation step covers all Au features in a SAM formed from a first thiol (PEG-terminated). Electrochemical desorption is then performed selectively by applying a desorbing potential to one feature (an arm of an MZI) while controlling the potential of the other features (other MZI arm and Y-junctions) to ensure SAM stability. The second incubation step then covers the desorbed regions (MZI arm) in a SAM formed from the second thiol (biotin-terminated), resulting in chemically differentiated regions. Although
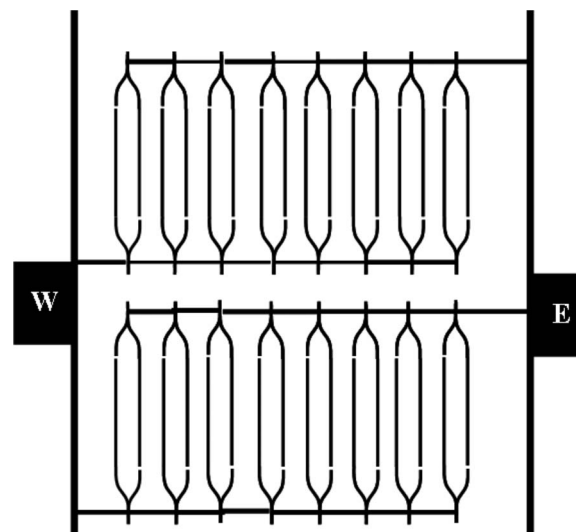
image in Fig. 10c, indicating the formation of SAM **II** on the empty Au stripe where SAM **I** had been selectively removed (e.g., Fig. 10a). Thus, both molecular mapping by TOF-SIMS and surface scanning by PS-AFM confirm the validity of the process to chemically differentiate the arms of an MZI.

Extension to wafer-scale processing.— The process is of greater usefulness when applied at the die or wafer scales to selectively treat many features simultaneously. For example, in the Au MZIs treated in this paper, the electrolysis step can be performed on many MZIs simultaneously by connecting west arms together to one contact pad denoted as "W," and likewise by connecting east arms together to another contact pad denoted as "E," as sketched in Fig. 11. Such an

Figure 11. Layout for die- or wafer-scale processing of Au MZI structures.

demonstrated here on plasmonic MZIs, the process can be applied generally to chemically differentiate a large number of electrically isolated Au features simultaneously, leading to low cost wafer-scale functionalization of (bio)chemical sensors and other devices.

References

1. P. Berini, R. Charbonneau, and N. Lahoud, *Nano Lett.*, **7**, 1376 (2007).
2. R. Charbonneau, M. Tencer, N. Lahoud, and P. Berini, *Sens. Actuators B*, **134**, 455 (2008).
3. P. Berini, *New J. Phys.*, **10**, 105010 (2008).
4. P. Berini, *Phys. Rev. B*, **61**, 10484 (2000).
5. A. W. Wark, H. J. Lee, and R. M. Corn, *Anal. Chem.*, **77**, 3904 (2005).
6. A. Kasry and W. Knoll, *Appl. Phys. Lett.*, **89**, 101106 (2006).
7. R. Slavík and J. Homola, *Sens. Actuators B*, **123**, 10 (2007).
8. S. Sidorenko and O. J. F. Martin, *Opt. Express*, **15**, 6380 (2007).
9. K. L. Prime and G. M. Whitesides, *Science*, **252**, 1164 (1991).
10. P. Harder, M. Grunze, R. Dahint, G. M. Whitesides, and P. E. Laibinis, *J. Phys. Chem. B*, **102**, 426 (1998).
11. E. Ostuni, R. G. Chapman, R. E. Holmlin, S. Takayama, and G. M. Whitesides, *Langmuir*, **17**, 5605 (2001).
12. M. Tencer, R. Charbonneau, N. Lahoud, and P. Berini, *Appl. Surf. Sci.*, **253**, 9209 (2007).
13. J. J. Ramsden, *Chem. Soc. Rev.*, **24**, 73 (1995).
14. M. Yang, F. L. Chung, and M. Thompson, *Anal. Chem.*, **65**, 3713 (1993).
15. J. Love, L. A. Estroff, J. K. Kriebel, R. G. Nuzzo, and G. M. Whitesides, *Chem. Rev. (Washington, D.C.)*, **105**, 1103 (2005).
16. S. H. Choi, J. W. Lee, and S. J. Sim, *Biosens. Bioelectron.*, **21**, 378 (2005).
17. K. E. Nelson, L. Gamble, L. S. Jung, M. S. Boeckl, E. Naeemi, S. L. Golledge, T. Sasaki, D. G. Castner, C. T. Campbell, and P. S. Stayton, *Langmuir*, **17**, 2807 (2001).
18. S. Busse, V. Scheumann, B. Menges, and S. Mittler, *Biosens. Bioelectron.*, **17**, 704 (2002).
19. M. Tencer, R. Charbonneau, and P. Berini, *Lab Chip*, **7**, 483 (2007).
20. M. Walczak, D. D. Popenoe, R. S. Deinhammer, B. D. Lamp, C. Chung, and M. D. Porter, *Langmuir*, **7**, 2687 (1991).
21. C. A. Widrig, C. Chung, and M. D. Porter, *J. Electroanal. Chem.*, **310**, 335 (1991).
22. D.-F. Yang, C. P. Wilde, and M. Morin, *Langmuir*, **12**, 6570 (1996).
23. X. Jiang, R. Ferrigno, M. Mrksich, and G. M. Whitesides, *J. Am. Chem. Soc.*, **125**, 2366 (2003).
24. A. K. Sheridan, P. Ngamukot, P. N. Bartlett, and J. S. Wilkinson, *Sens. Actuators B*, **117**, 253 (2006).
25. M. Tencer and P. Berini, *Langmuir*, **24**, 12097 (2008).
26. A. Benninghoven, *Angew. Chem., Int. Ed. Engl.*, **33**, 1023 (1994).
27. D. J. Graham and B. D. Ratner, *Langmuir*, **18**, 5861 (2002).
28. S. C. C. Wong, N. P. Lockyer, and J. C. Vickerman, *Surf. Interface Anal.*, **37**, 721 (2005).
29. J. P. Cleveland, B. Anczykowski, A. E. Schmid, and V. B. Elings, *Appl. Phys. Lett.*, **72**, 2613 (1998).
30. F. Martínez and R. García, *Nanotechnology*, **17**, S167 (2006).
31. H.-Y. Nie, J. T. Francis, A. R. Taylor, M. J. Walzak, W. H. Chang, D. F. MacFabe, and W. M. Lau, *Appl. Surf. Sci.*, **255**, 1079 (2008).
32. M. Tencer, *Microelectron. Reliab.*, **48**, 584 (2008).
33. T. K. Trunova, *Glass Ceram.*, **31**, 329 (1974).
34. V. S. Golovin and V. G. Zheltov, *Glass Ceram.*, **34**, 489 (1977).
35. M. El Sherbiny, in *Proceedings of the 37th IEEE Midwest Symposium on Circuits and Systems*, p. 1281 (1994).
36. Y. L. Chow, M. M. Elsherbiny, and M. M. A. Salama, *IEE Proc.: Gener. Transm. Distrib.*, **142**, 653 (1995).
37. http://www-ec.njit.edu/~grow/conductivity.htm, last accessed October 2009.
38. C. S. Tang, M. Dusseiller, S. Makohliso, M. Heuschkel, S. Sharma, B. Keller, and J. Voros, *Anal. Chem.*, **78**, 711 (2006).
39. L. M. Tender, K. A. Opperman, P. D. Hampton, and G. P. Lopez, *Adv. Mater.*, **10**, 73 (1998).
40. M. Tencer, H.-Y. Nie, and P. Berini, Submitted.
41. P. Achalla, J. McCormick, T. Hodge, C. Moreland, P. Esnault, A. Karim, and D. Raghavan, *J. Polym. Sci., Part B: Polym. Phys.*, **44**, 492 (2006).
42. M. Kober, E. Sahagun, M. Fuss, F. Briones, M. Luna, and J. J. Saenz, *Phys. Status Solidi (RRL)*, **2**, 138 (2008).